



The lithosphere–asthenosphere boundary and the tectonic and magmatic history of the northwestern United States



Emily Hopper^{a,*}, Heather A. Ford^{a,1}, Karen M. Fischer^a, Vedran Lekic^b,
Matthew J. Fouch^c

^a Department of Geological Sciences, Brown University, 324 Brook St., Providence, RI 02912, USA

^b Department of Geology, University of Maryland, College Park, MD, USA

^c Department of Terrestrial Magmatism, Carnegie Institution of Washington, Washington, DC, USA

ARTICLE INFO

Article history:

Accepted 12 December 2013

Available online 15 January 2014

Editor: P. Shearer

Keywords:

scattered waves

lithosphere

lithosphere–asthenosphere boundary

mid-lithospheric discontinuity

ABSTRACT

This study explores the properties of the lithosphere–asthenosphere boundary (LAB) and other shallow mantle discontinuities across the diverse geologic provinces of the northwest United States. Sp phases were used to image three-dimensional discontinuity structure by common conversion point stacking with data from 804 temporary and permanent broadband stations, including 247 from EarthScope's USArray Transportable Array. Substantial variations in mantle discontinuity structure are apparent over a variety of spatial and temporal scales. To the west of the Sevier Thrust Belt, a coherent Sp negative phase coincides with the LAB depth range inferred from tomographic models. To the east, within the stable craton, multiple negative phases typically occur in the high velocity lithospheric layer, although in places a single mid-lithospheric discontinuity is imaged. Sub-cratonic LAB phases are often absent, indicating an LAB velocity gradient that is distributed over >50 km and that is consistent with effects of temperature alone. Where weak and intermittent LAB phases appear, they suggest more vertically localized velocity gradients produced by other factors such as bulk composition, volatile content, or contrasts in grain size or melt. In the tectonically active west, a positive Sp phase at depths consistent with the base of the asthenospheric low velocity zone in tomography models is intermittently observed. Beneath magmatic provinces in the west, the LAB Sp discontinuity deepens by ~10 km from the High Lava Plains, where magmatism has occurred from 0–10.5 Ma, to the northern region of the Columbia River Basalts, which has been magmatically quiet since 15 Ma. Here we suggest a model in which the negative LAB velocity gradient is created by a layer of partial melt ponding beneath a solidus-defined boundary. This model predicts that higher temperatures associated with more recent magmatism would result in a shallowing of the intersection of the geotherm with the solidus. Beneath the Yellowstone Caldera, the absence of an LAB Sp phase suggests that the contrast in seismic velocity between the lithosphere and asthenosphere has been erased by intrusion of partial melt and heat into the lithosphere.

© 2013 Elsevier B.V. All rights reserved.

1. Introduction

1.1. The lithosphere–asthenosphere boundary

The lithosphere is classically defined rheologically and kinematically as the rigid plate that translates coherently with surface plate motions. In this study we probe the properties of the mantle portion of the lithosphere as defined by its seismic wavespeed, i.e. the high velocity layer above the asthenospheric low velocity zone.

The primary mechanisms for the velocity decrease from lithosphere to asthenosphere are temperature, volatile content, bulk

composition, partial melt, grain size, and anisotropic fabrics, all of which can be reset by tectonic and magmatic processes. Here we image the seismologically-defined lithosphere–asthenosphere boundary (LAB) and other shallow mantle discontinuities across the diverse geologic provinces of the northwest United States. Our goal is to better understand the mechanisms responsible for producing the seismically observed LAB and how the LAB and other mantle discontinuities relate to the region's tectonic and magmatic evolution.

1.2. Tectonic and magmatic setting and prior studies of seismological structure

The tectonic and magmatic evolution of the northwestern United States is expressed over several different temporal and spatial scales. At the broadest scales, our study region is divided along the Sevier Thrust Belt into a western region that

* Corresponding author. Tel.: +1 401 863 1965.

E-mail address: Emily_Hopper@brown.edu (E. Hopper).

¹ Now at Department of Geology and Geophysics, Yale University, New Haven, CT, USA.

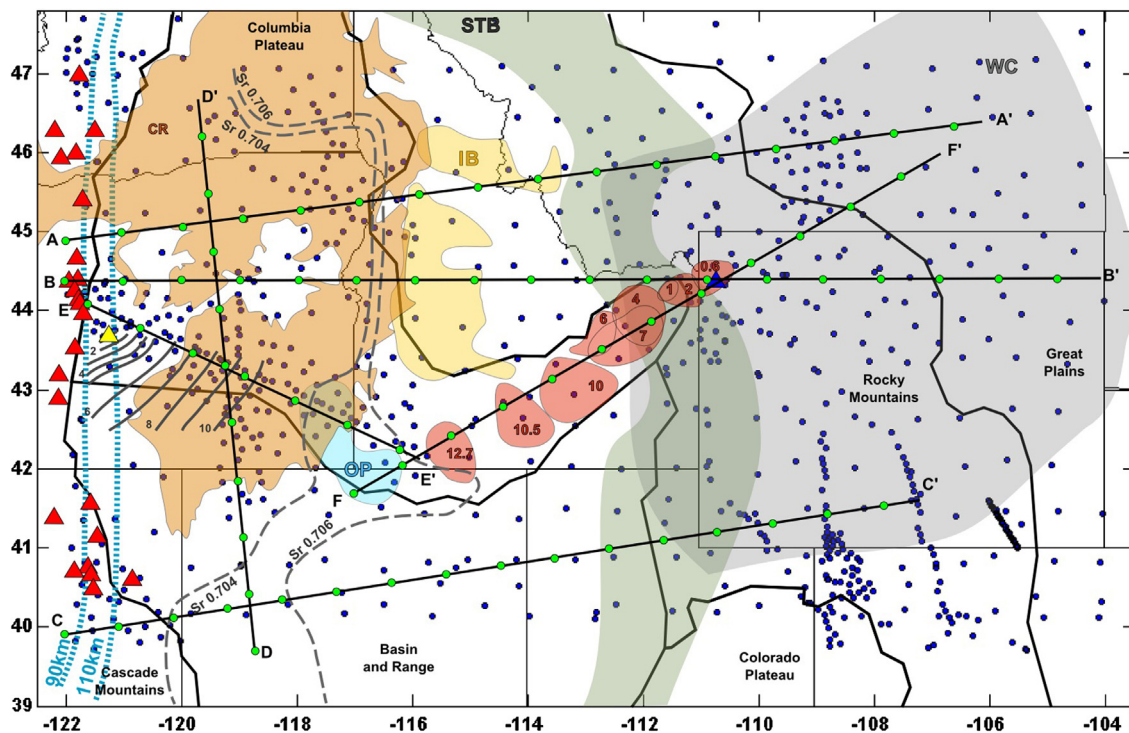


Fig. 1. Map of the study area. Thick black lines with green circles: cross-section locations. Dark blue circles: broadband stations that contributed data to this study. Red triangles: arc volcanoes. Yellow triangle: Newberry Volcano. Blue triangle: Yellowstone Caldera. Red shaded areas: rhyolitic calderas in the eastern Snake River Plain, with age in Ma, after Smith et al. (2009). Grey shaded area (WC): Wyoming Craton, after Foster et al. (2006). Green shaded area (STB): Sevier fold and thrust belt, after DeCelles and Coogan (2006). Orange shaded area (CR): Columbia River flood basalts and Steens basalts, after Camp and Ross (2004). Yellow shaded area (IB): Idaho Batholith, after Gaschnig et al. (2011). Blue shaded area (OP): Owyhee Plateau, after Shoemaker (2004). Dashed grey lines (Sr 0.704 and Sr 0.706): Sr lines, after Eagar et al. (2011). Solid grey lines: isochrons showing age progression of the High Lava Plains silicic volcanism, labeled with earliest age in Ma, after Eagar et al. (2011). Hatched light blue lines: contours of depth to top of Juan de Fuca slab, labeled with depth, after McCrory et al. (2006). Thick black lines: boundaries between tectonic provinces, labeled in black, from Fenneman and Johnson (1946). (For interpretation of the references to color in this figure legend, the reader is referred to the web version of this article.)

has experienced significant deformation and magmatic activity throughout the Phanerozoic, and an eastern region where deformation has been less extensive, particularly in the last 50 My (Fig. 1). The Archean Wyoming Craton forms the core of the eastern region, though there are also other ancient, stable continental blocks, including the Medicine Hat Block and the Colorado Plateau (Foster et al., 2006; Fig. S3). The ancient continental blocks extending several hundreds of kilometers west of the Sevier Thrust Belt – i.e. the Paleoproterozoic Selway Terrane and Archean Grouse Creek Block – underwent greater degrees of tectonic and magmatic reworking (Foster et al., 2006). These blocks are bounded on the west by Phanerozoic accreted terranes, a boundary often associated with strontium isopleths, with $^{87}\text{Sr}/^{86}\text{Sr}$ decreasing westwards (Armstrong et al., 1977; Coney et al., 1980).

Phanerozoic tectonism was dominated first by subduction and orogenesis. Convergence has included the Cretaceous to Eocene Sevier and Laramide Orogenies. While the Sevier Thrust Belt marks the eastern limit of the Sevier Orogeny, Laramide deformation extended further east, building the Rocky Mountains (Dickinson, 2004; Saleeby, 2003; Tikoff and Maxson, 2001). By the Early Miocene, part of the convergent boundary on the continental margin had converted to the San Andreas transform. Consequent Basin and Range extension is estimated to have reached values of 50% or more within the study area (Dickinson, 2004; McQuarrie and Wernicke, 2005).

One feature common to many recent tomography models is the marked transition from shallow upper mantle with low seismic velocities in regions that have experienced high degrees of tectonic reworking and magmatism to a thick, high velocity mantle layer elsewhere (e.g. Burdick et al., 2012; Darold and Humphreys,

2013; James et al., 2011; Obrebski et al., 2011; Schmandt and Humphreys, 2010; Shen et al., 2013; Sigloch, 2011; Yuan et al., 2011). South of $\sim 45^\circ$ N, this transition appears at the eastern margin of the Basin and Range and Snake River Plain, with the exception of lower velocity upper mantle beneath the High Rockies south of the Wyoming Craton. In the northern portion of our study region, the transition typically occurs further west at longitudes of 118° – 119° W.

The region has experienced a long and varied magmatic history. The Columbia River Flood Basalts, emplaced between 16.6 and 15.0 Ma (Camp et al., 2003; Hooper et al., 2002), outcrop in the northwest of the study region (Fig. 1). Their southern lobe was overprinted by later High Lava Plains volcanism. In the High Lava Plains, a wave of silicic volcanism started at ~ 15.5 Ma and has propagated towards the northwest (e.g. Jordan et al., 2004). Recent work extends this trend into the northwest Basin and Range to 12 Ma (Ford et al., 2013). Along the eastern Snake River Plain, silicic volcanics decrease in age from 12–0 Ma in the direction opposite to North American plate motion, culminating in the active volcanism beneath Yellowstone Caldera (e.g. Christiansen et al., 2002; Pierce and Morgan, 2009, 1992; Shervais and Hanan, 2008). In both the High Lava Plains and eastern Snake River Plain, basaltic magmas have erupted since 10.5 Ma with no age-progressive trend (e.g. Christiansen et al., 2002; Jordan et al., 2004; Till et al., 2013a).

In the High Lava Plains area, low velocities are observed to shallow mantle depths, implying small lithospheric thicknesses (Wagner et al., 2010; Obrebski et al., 2011; Hanson-Hedgecock et al., 2012; Gao and Shen, 2014). Furthermore, temperatures and pressures of basaltic melt equilibration indicate that as-thenospheric conditions exist at very shallow mantle depths

(Till et al., 2013a). The upper limit on crustal extension in the High Lava Plains, constrained by paleomagnetic and crustal thickness observations, is 16–17% (Eagar et al., 2011; Wells and Heller, 1988); some postulate advective and convective thinning instead (Long et al., 2012).

The Yellowstone–Snake River Plain volcanic trend lies above the most prominent low velocity mantle anomaly in the western United States, a low velocity channel extending to depths of ~200 km (e.g. Burdick et al., 2012; Obrebski et al., 2011; Schmandt and Humphreys, 2010; Shen et al., 2013; Sigloch, 2011; Wagner et al., 2010). Regardless of the ongoing debate as to the cause and depth extent of this anomaly (e.g. Fouch, 2012; James et al., 2011; Obrebski et al., 2011; Schmandt and Humphreys, 2010; Schmandt et al., 2012), it is clear that the lithosphere beneath the Snake River Plain has been heavily altered. Yellowstone–Snake River Plain magmatism is particularly interesting in this study as the silicic calderas have distinctly different ages. Thus, we can examine magmatic interactions with the lithosphere at small spatial (<100 km) and temporal (~1 Ma) scales.

A wide variety of models have been proposed to explain the magmatic history of the northwestern United States (see Long et al., 2012 for a summary). Recently, models of subduction zone flow and, in some cases, its interaction with a mantle plume have been developed for the region (Druken et al., 2011; Faccenna et al., 2010; Kincaid et al., 2013; Liu and Stegman, 2012; Long et al., 2012) in response to the magmatic trends and tomographic results described above, and constraints on mantle anisotropy (Lin et al., 2011; Long et al., 2009; Yuan and Romanowicz, 2010b).

A goal of this study is to better understand how the continental lithosphere responds to tectonic and magmatic re-working by examining how shallow (<200 km) mantle discontinuity structure varies between cratonic and non-cratonic regions, and between non-cratonic regions with different magmatic histories. Due to their enhanced sensitivity to vertical velocity gradients, scattered waves such as Sp are an important complement to the constraints on volumetric heterogeneity provided by tomography. For example, while surface wave tomography typically cannot distinguish vertical velocity gradients over 50–70 km from those over smaller depth ranges, Sp phases at dominant periods of ~10 s will typically be clearly observed for velocity changes of less than ~8% only if they occur over less than ~30 km in depth (e.g. Ford et al., 2010; Rychert et al., 2007). Conversely, if tomography shows that a significant (>4%) velocity gradient occurs but Sp phases are not observed, the velocity gradient must be distributed over a depth range of ~50 km or more.

A number of recent studies have used Ps and Sp phases to examine the western United States (Abt et al., 2010; Eagar et al., 2011; Hansen et al., 2013; Kumar et al., 2012; Lekic and Fischer, 2014; Lekic et al., 2011; Levander and Miller, 2012; Levander et al., 2011; Li et al., 2007; Schmandt et al., 2012; Sheehan et al., 2000). Of these, several have investigated upper mantle discontinuities in study regions overlapping the one considered here (Abt et al., 2010; Kumar et al., 2012; Lekic and Fischer, 2014; Levander and Miller, 2012; Li et al., 2007). Advantages provided by our study include a greater density of data over the study area; a new technique for more accurate automated phase picking (Lekic and Fischer, 2014) that allows more waveforms to be more correctly incorporated; a bandpass filter that minimizes interference between adjacent phases; and bootstrapping of the Sp-based image to determine which phases are robust.

One of the major results of these previous studies was Levander and Miller's (2012) observation of a pronounced change in depth of their observed phases across the Sevier Thrust Belt. We confirm this observation, and further explore the fundamental change in discontinuity character across this boundary. Furthermore, we observe pronounced variations in apparent lithospheric thickness

between magmatic provinces of different ages. For example, the phase beneath the Columbia River is observed to be deeper than that beneath the High Lava Plains and northern Basin and Range. We also note the absence of a strong negative phase beneath the Moho in the vicinity of the active Yellowstone Caldera.

2. Data and methods

2.1. Sp waveforms

To avoid complications from crustal reverberations, we imaged shallow mantle discontinuities with Sp phases. S waveforms were obtained from the Incorporated Research Institutions for Seismology (IRIS) Data Management Center for events in the USGS National Earthquake Information Center catalog with $M_w > 5.8$. Data from all available broadband stations (804 stations from 31 permanent and temporary networks) within a ~1500 km by ~900 km region centered on the eastern Snake River Plain (Fig. 1) were employed. Included are 247 Earthscope USArray Transportable Array stations, which crossed the area between 2006 and 2010; 118 High Lava Plains stations, which operated between 2006 and 2009; and 19 permanent stations of the U.S. National Seismic Network and IRIS Global Seismic Networks, some providing data for as many as 20 years. At short epicentral distances, Sp waves turn post-critical at larger depths; the critical depth increases with increasing epicentral distance. Based on the coherence of the final images, we found a distance range of 55–85° and the exclusion of sources below 300 km (e.g. Wilson et al., 2006) to be the best compromise between reducing contamination and adding more data. Our stacks include 77,671 waveforms sourced from 1377 events with an uneven coverage distribution, matching the variable station distribution (Fig. 2; Fig. 1). In our dataset, the earthquakes are primarily located in the South American subduction zone, to the southeast of the study area, and in the Aleutian and Japan subduction zones, to the northwest. This strong back-azimuthal bias creates the southeast–northwest banding in the distribution of the number of phases contributing to CCP stack (Fig. 2).

To identify S phase windows for analysis, we used the automated array-based procedure of Lekic and Fischer (2014). We employed a free surface transfer matrix to rotate the recorded wavefield into its P and SV components, suppressing the effects of the free surface (Bostock, 1998; Kennett, 1991). An automated search was performed over V_p and V_p/V_s space to find the free-surface values that minimize the amplitude of the parent phase, SV, on the daughter component, P (e.g. Abt et al., 2010).

2.2. Deconvolution, migration, stacking and bootstrapping

For each event-station pair, we deconvolved the P from the SV component using the extended-time multi-taper cross-correlation method (Helffrich, 2006) with the deconvolution parameters of Lekic and Fischer (2014).

We migrated the deconvolved waveforms into a three-dimensional volume and stacked them with a common convergent point (CCP) approach and a spline function representation of the Sp Fresnel zone, more completely described in Lekic et al. (2011). Sp times were corrected for lateral heterogeneity by ray-tracing through station averages of the crustal model of Lowry and Pérez-Gussinyé (2011) and mantle P-wave and S-wave velocities from Obrebski et al. (2011, 2010). The Fresnel zones used were based on the dominant period of the waves; with the 4–33 s filter used for the images in this paper, we measured a dominant period of 9 s for the waveforms. We excluded energy from depths where conversions are expected to be post-critical. We also reversed the polarity of the recorded phases to facilitate comparison with Ps phase results.

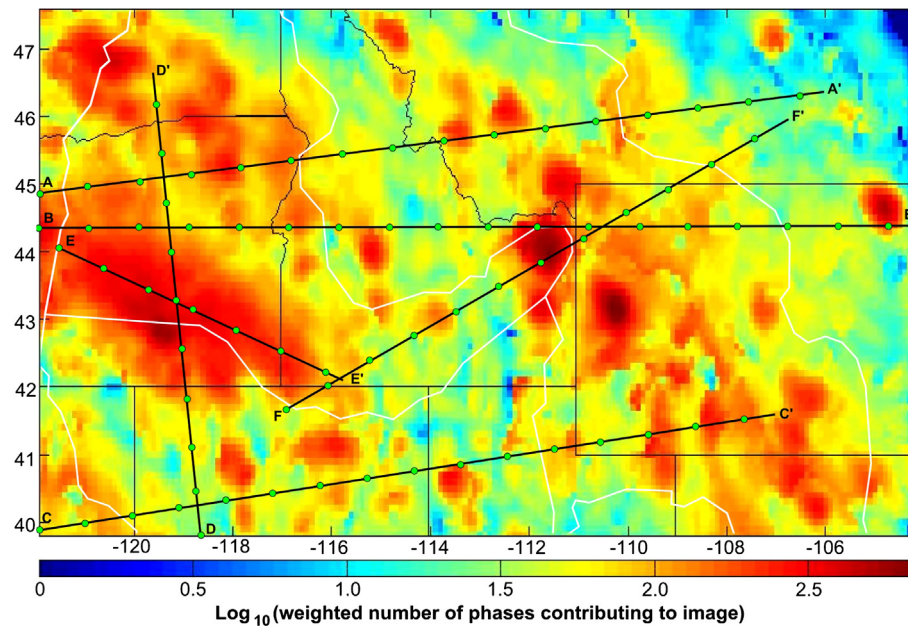


Fig. 2. Spatial distribution of Sp phases. Logarithmically scaled plot of the number of phases contributing to the Sp CCP stack at a given point, taking into account the weighting factor applied to each phase by the spline function representation of its Fresnel zone (Lekic et al., 2011). Values are taken from the depth at which the strongest negative phase was automatically picked. Where no phase was picked, the value is taken from the mean depth of all phases picked over the entire study area.

To assess the robustness of the phases observed in the Sp CCP stack, we calculated 50 versions of the stack each based on a different random sample of the Sp waveforms, as well as the mean and standard deviation of the 50 stacks. Figures shown in the main text of this paper all derive from the mean of the bootstrapped stack. Phases observed in the bootstrapped stack are very similar to those in the image based on the complete dataset, particularly in the western portion of the study region where a single clear mantle Sp phase is typically observed. In the east, where multiple mantle phases at different depths are common, comparable phases are observed in the bootstrapped stack and the stack containing all waveforms, although phase amplitudes sometimes differ (Supplementary Materials).

2.3. Discontinuity depths and uncertainties

The depth of the negative phase beneath the Moho was picked automatically as the mean depth of the 25 most negative points in the 35–200 km depth range, as described in Lekic et al. (2011). Uncertainties in phase depth are a product of a) the scatter in the observed Sp waveforms, b) errors in the velocity model used to migrate the phases from time into the CCP stack volume, and c) the finite width of the phase peak and its interference with adjacent arrivals, both of which increase with longer dominant periods. Experimentation with different bandpass filters indicated the least interference between adjacent phases was achieved using a filter with a low frequency corner of 0.25 Hz or greater (Supplementary Materials). In the western half of our study region, uncertainties in phase depth from bootstrap testing (one standard deviation) are less than 5 km over ~70% of the area; in the eastern half, this drops to ~40% of the area (Fig. S1). Due to the high quality crust and mantle models used to correct for lateral heterogeneity, uncertainties due to lateral heterogeneity will be <5 km for depths less than 150 km (e.g. Lekic et al., 2011). In the western half of our study region, where we interpret mantle Sp phase depths, net depth uncertainties are typically less than ~10 km.

3. Observed mantle discontinuities and their origin

We observe negative Sp phases at mantle depths throughout much of the study region. As we reversed Sp polarity to match the Ps sign convention, this negative phase corresponds to a velocity decrease with depth. Based on comparison of the depth of this phase to the high velocity lid seen in tomography (e.g. Obrebski et al., 2011; Wagner et al., 2010), the negative phase is classified as a lithosphere–asthenosphere boundary phase (LAB) if it is at least as deep as the mid-point between the peak velocity in the high velocity lid and the minimum velocity in the low velocity layer beneath. The phase is deemed a mid-lithospheric discontinuity (MLD) if it falls at depths shallower than this mid-point.

In general, we observe variations in the Sp phase properties between different tectonic provinces over a variety of spatial and temporal scales. At the longest spatial and temporal scales, pronounced differences in discontinuity character exist between the highly deformed region west of the Sevier Thrust Belt and the thicker, more stable lithosphere to its east. At smaller scales, differences in negative discontinuity depth are observed between the 16 Ma Columbia River Basalts and the High Lava Plains and the northwest Basin and Range, where more recent magmatism has occurred. At the shortest scales, the seismological LAB appears to have been completely disrupted beneath the youngest Yellowstone caldera with its active magmatism.

3.1. Cratonic lithosphere

3.1.1. Cratonic vs. more recently tectonized lithosphere

To the west of the Sevier Thrust Belt, a strong negative phase is commonly observed. South of 45° N this phase can be interpreted as the seismological LAB, based on comparisons of phase depth with tomography described earlier; north of 45°, clear association of this phase with the LAB becomes possible west of ~119° W. In contrast, in the cratonic regions to the east of the Sevier Thrust Belt, weaker MLD phases are observed. In some areas a single MLD phase dominates the CCP stack, but often multiple MLD phases appear at different depths within the thick high velocity cratonic

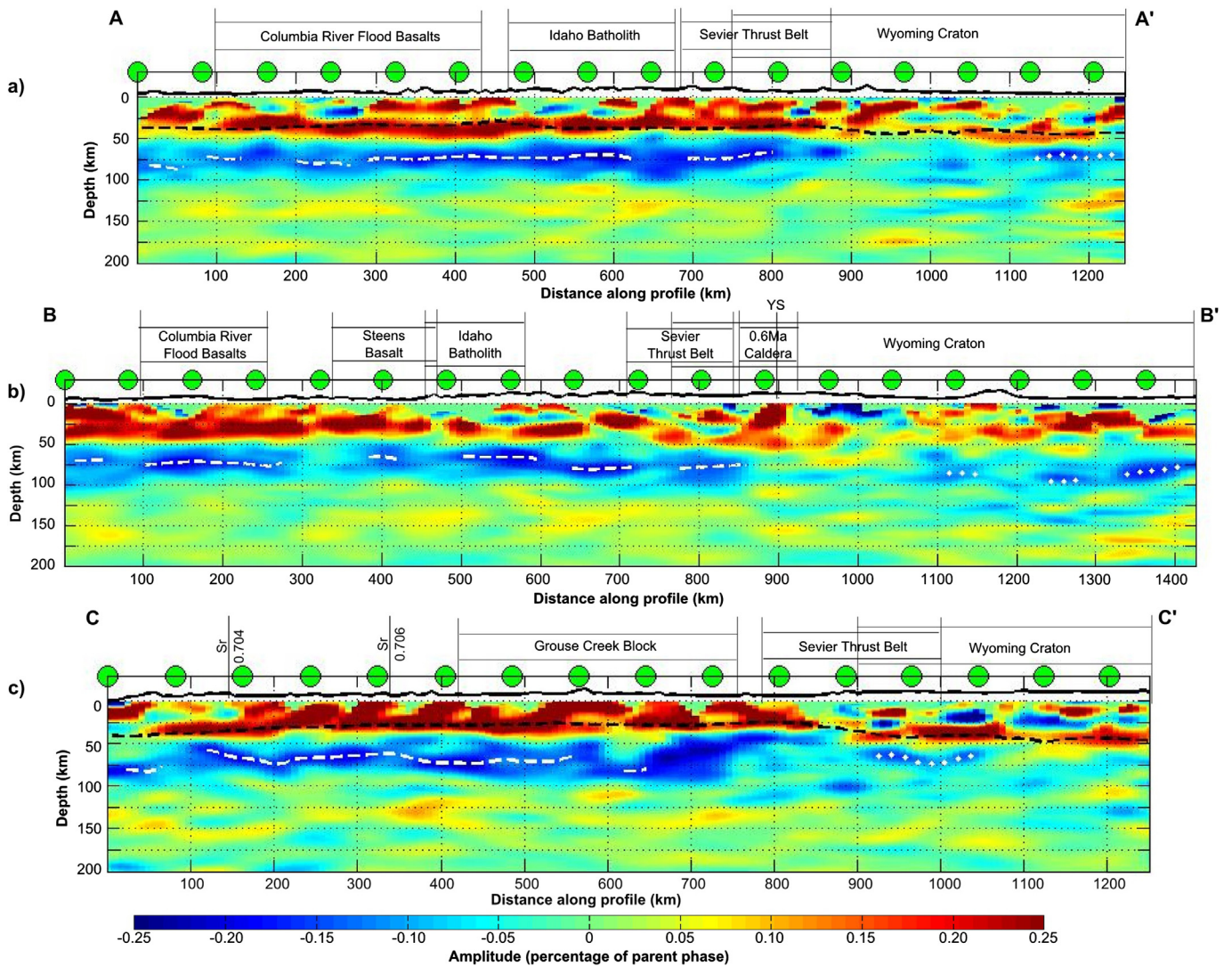


Fig. 3. Cross-sections through mean of bootstrapped Sp CCP stack. Cross-section locations shown in Fig. 1 with corresponding green circles. Where fewer than 35 unweighted paths contribute to a model point, zero amplitude is plotted. a) Cross-section A–A' runs from 44.9° N, 122° W to 46.4° N, 106.1° W. b) Cross-section B–B' runs from 44.4° N, 122° W to 44.4° N, 104° W. c) Cross-section C–C' runs from 39.9° N, 120.7° W to 41.6° N, 107.3° W. In all plots, CCP stack is from data filtered at 4–33 s, with a dominant period of 9 s. Thick black line: topography, at 5× vertical exaggeration. Dashed black line: Moho (Lowry and Pérez-Gussinyé, 2011). Dashed white line: auto-picked negative phase, interpreted as LAB. Dotted white line: auto-picked negative phase, interpreted as MLD. Labels above sections give approximate locations of surface features.

lithosphere. The contrast in mantle discontinuity character across the Sevier Thrust Belt is evident on profiles that cross the western edge of the Archean Wyoming Craton (Profiles A–C, Fig. 3), although additional perturbations due to the Yellowstone hotspot track must also be considered (Profile B, Fig. 3), as discussed in the next section. Strong laterally continuous negative phases within the potential LAB depth range are not observed beneath cratonic regions, although weak negative, intermittent phases sometimes occur at LAB depths. MLD phases within the cratonic lithosphere are almost exclusively negative, i.e. they appear to originate at a velocity decrease with depth. This observation may reflect real velocity structure, e.g. a series of velocity decreases or alternating velocity decreases and increases where the decreases are vertically localized and the increases are too distributed in depth to produce sharp phases. However, another possibility is that interference between phases from multiple discontinuities obscures aspects of the velocity gradient structure.

The change from a coherent LAB phase in the west to distributed MLDs within the craton does not correlate with a decrease in the density of contributing Sp phases. For example, in western regions of cross-section C–C' (Fig. 3), a clear LAB is seen despite

relatively sparse data collected largely from TA stations. In contrast, beneath the Wyoming craton where the distributed phase is observed, the TA is augmented by several temporary PASSCAL deployments (i.e. Deep Probe, CD-ROM, Lodore, Laramie), and more waveforms contribute to the image at a given node.

Given the distributed nature of the phase in the cratonic east, it can be misleading to make comparisons on the basis of depth and strength of a single phase between these two regions. Nonetheless, maps of the mean depth and amplitude of the strongest negative phases autopicked from the bootstrapped Sp CCP stacks (Fig. 4) provide a useful synoptic view. Among the distributed MLD phases within cratonic regions to the east of the Sevier Thrust Belt, the largest phase is typically deeper (>80 km) and lower amplitude than the phases interpreted as the LAB in the west. In the amplitude map (Fig. 4b) the translucent white mask indicates areas where fewer than 50 weighted waveforms contribute to the image at a given model node. In these portions of the image, an artificial bias that enhances amplitude exists. Phase depth is more robust than phase amplitude in these zones, although these depths should still be viewed with greater skepticism than those where there is better sampling.

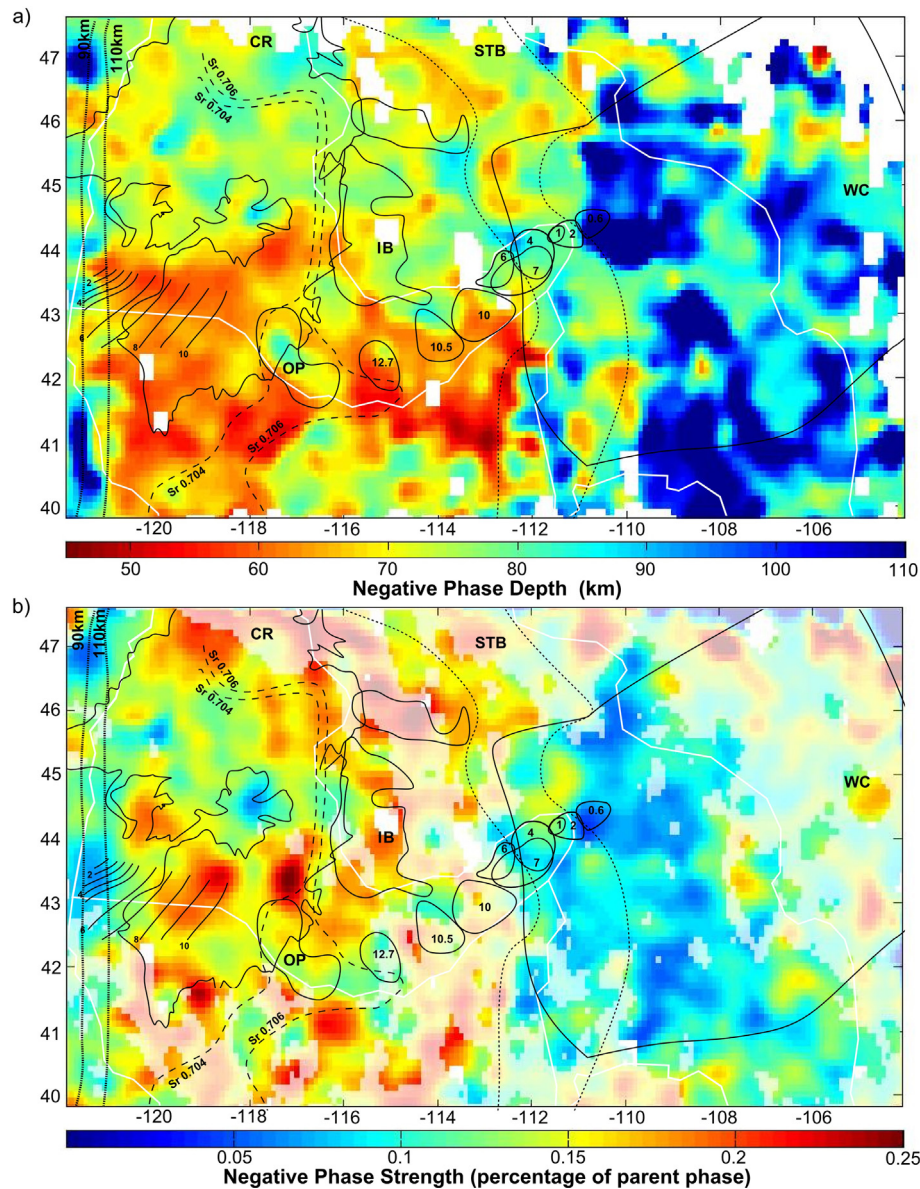


Fig. 4. Mean depth and amplitude of largest negative Sp phase in the 50 bootstrapped stacks, as picked by automated picker. While maps appear to be showing variation in a single interface, the interpretation of the negative phase changes across the region. No value is given (i.e. pixel is white) where the phase was too weak to be picked. White lines: boundaries between tectonic provinces, as in Fig. 1. Black lines: smaller scale tectonic features, labeled as in Fig. 1. a) Depth map. b) Amplitude map. Translucent white mask indicates areas where fewer than 50 weighted waveforms contribute to the image at a given model node.

A comparable contrast in discontinuity character between cratonic and non-cratonic regions was also observed in the western U.S. to the south of our study region by [Lekic and Fischer \(2014\)](#) who used methods identical to those of this study. A change in the amplitude and depth of the largest negative phase across the Sevier Thrust Belt was first documented by [Levander and Miller \(2012\)](#), although aspects of their images, phase-picking approach and interpretation differ from ours. Broadly speaking, a deepening of the largest negative phase across the Sevier Thrust Belt also appears in the images of [Kumar et al. \(2012\)](#).

3.1.2. The origin of layering within the cratonic lithosphere

The variable number of mantle discontinuities within the lithosphere of the Wyoming craton indicates layering within the cratonic lithosphere, some of which is dipping or laterally discontinuous. Models for the formation of the cratonic mantle lithosphere include underthrusting and stacking of oceanic lithosphere (e.g. [Canil, 2008, 2004](#); [Lee, 2006](#); [Lee et al., 2011](#); [Simon et](#)

[al., 2007](#)); thickening of arc lithosphere ([Kelemen et al., 1998](#); [Lee, 2006](#); [Lee et al., 2011](#); [Parman et al., 2004](#)); and a two-stage process involving growth of a “thermal blanket” at the base of an original highly depleted lithospheric layer ([Cooper et al., 2004](#); [Yuan and Romanowicz, 2010a](#)). The formation of cratonic mantle lithosphere as the residue of melting in large plume heads has also been proposed, but would predict compositions for cratonic peridotites consistent with high degrees of melting at large depths. As observed compositions suggest a low pressure origin ([Lee, 2006](#); [Lee et al., 2011](#)), we focus on the first three mechanisms. Of these, the lateral scale of the observed MLDs are most reminiscent of the imbrication of oceanic slab fragments, although this model would be more clearly supported if the MLDs were geometrically linked to sutures within the crust, as is the case with anisotropic Ps discontinuities in the Slave craton ([Bostock, 1998](#); [Mercier et al., 2008](#); [Snyder, 2008](#)). Accretion of depleted mantle from beneath island arcs seems less likely to produce discontinuities that are laterally continuous over hundreds of kilometers,

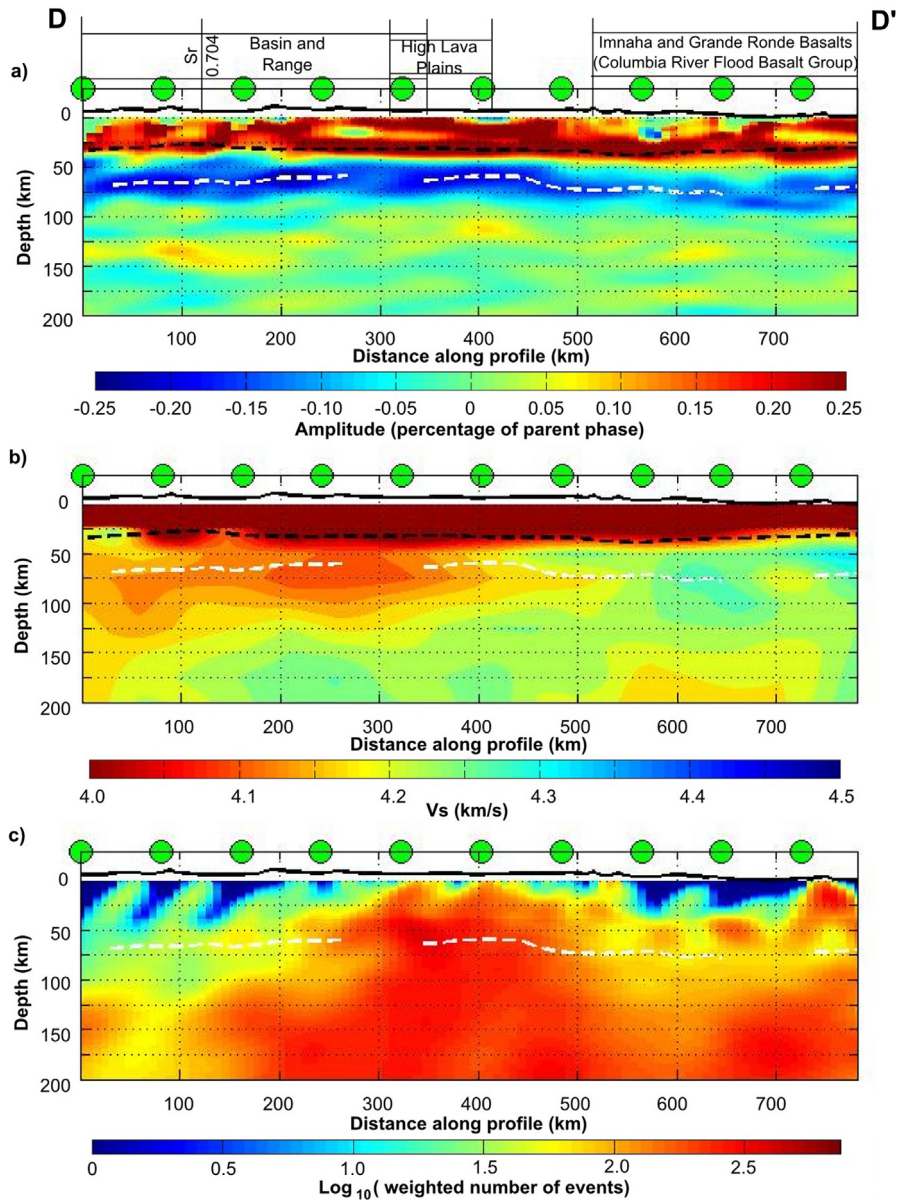


Fig. 5. a) Cross-section D–D' through mean of bootstrapped Sp CCP stack (4–33 s). b) Corresponding cross-section through the tomography model of Obrebski et al. (2011). c) Cross-section of the weighted number of phases contributing to the image. Cross-section runs from 39.7° N, 118.7° W to 46.7° N, 119.7° W. Thick black line: topography, at 5× vertical exaggeration. Dashed black line: Moho (Lowry and Pérez-Gussinyé, 2011). Dashed white line: auto-picked negative phase, interpreted as LAB.

as observed in parts of the craton; geodynamic modeling would be required to verify this point. On the other hand, the observed MLDs are more laterally variable than the two craton-wide lithospheric layers implied by the “thermal blanket” model (Cooper et al., 2004), although the relationship of the Sp-derived discontinuities and the vertical layering in azimuthal anisotropy used by Yuan and Romanowicz (2010a) in support of this model remains to be systematically explored.

3.2. Lithosphere to the west of the Sevier Thrust Belt

3.2.1. Columbia river flood basalts, the High Lava Plains and the northwest Basin and Range

Within the western, more recently tectonized portion of the study region, the depth of the LAB as defined by the Sp CCP stack shows pronounced variations at the boundaries of major magmatic provinces. Beneath the High Lava Plains, with its well-defined 0–10 Ma age-progressive silicic magmatic trend, and the adjacent northwest Basin and Range into which the age-progressive mag-

matism extends to a latitude of $\sim 42.25^\circ$ (Ford et al., 2013), a clear LAB phase lies at depths between 55 and 65 km (Figs. 4, 5 and 6). However, a distinct deepening of the phase (10 km or more) occurs moving north across the boundary of the High Lava Plains with the northern lobe of the Columbia River Basalts, where significant magmatism has not occurred since ~ 15 Ma (Hooper et al., 2002). This deepening is consistent with the ambient noise tomography of Gao and Shen (2014).

Beneath much of the High Lava Plains, a very strong and clear negative Sp phase is observed (Fig. 6). The phase depth falls at the top of the low velocity asthenospheric layer seen in tomography models (Obrebski et al., 2011; Wagner et al., 2010), so we interpret it as the LAB. The combination of the Sp phase and the tomography indicate that a thin, high velocity mantle lid is present and possibly thickens slightly in the direction of the older silicic volcanism. The amplitude of the phase diminishes beneath the youngest magmatic ages at the northwest end of the age-progressive trend, including Newberry volcano (Fig. 6); phase amplitudes are also typically low beneath the Cascades arc (Fig. 4; Fig. S7). It is tempting to suggest

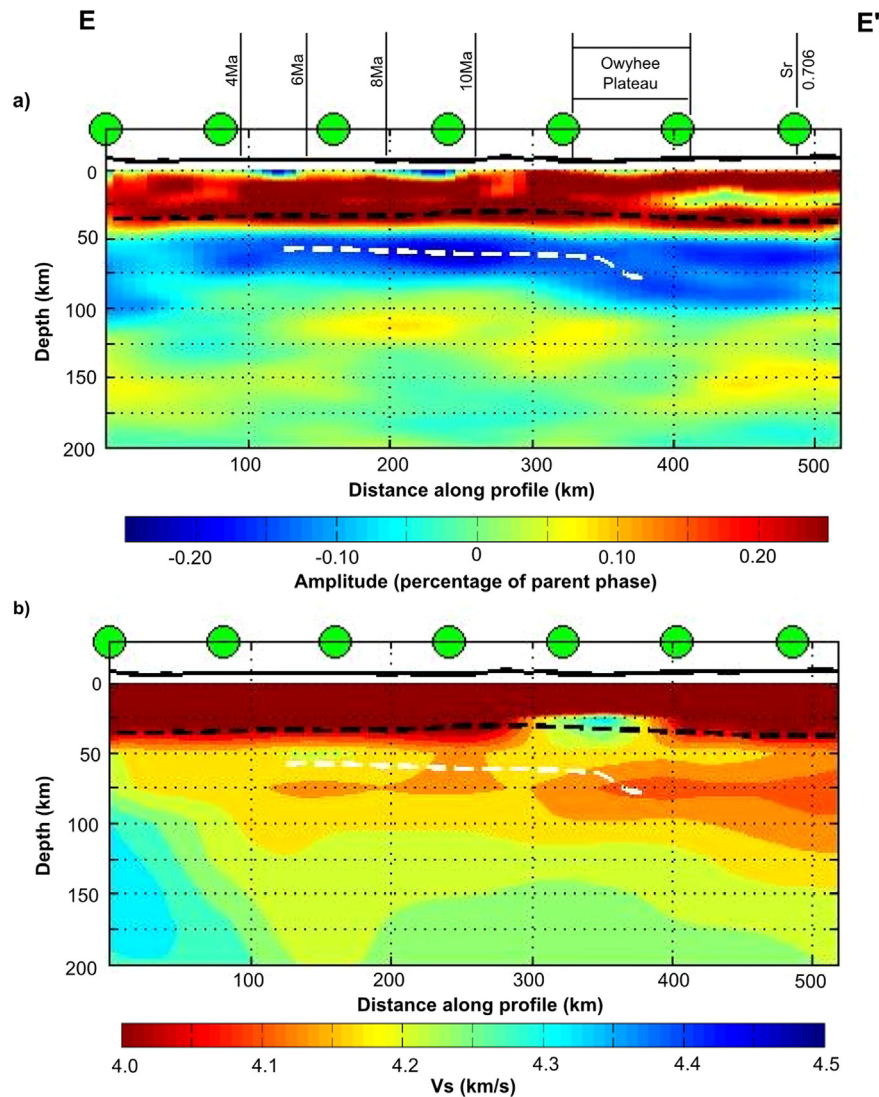


Fig. 6. a) Cross-section E–E' through mean of bootstrapped Sp CCP stack (4–33 s). b) Corresponding cross-section through the tomography model of Obrebski et al. (2011). Cross-section runs from 44.11° N, 121.589° W to 42.142° N, 115.808° W. Thick black line: topography, at 5× vertical exaggeration. Dashed black line: Moho (Lowry and Pérez-Gussinyé, 2011). Dashed white line: auto-picked negative phase, interpreted as LAB.

that in these volcanically active regions magmas and associated heat are abundant enough to significantly reduce velocities within the mantle lid and nearly erase any decrease in velocity at the LAB. However, interference between a potential LAB Sp phase and phases arising across the top of the subducting slab, which lies at depths of 90–100 km in this vicinity, may also be a factor (Fig. S7).

In the High Lava Plains, the observed depth of the Sp-defined LAB (ranging from 55–65 km, with uncertainties of ~10 km) is approximately consistent with the depths of last equilibration of asthenospherically derived basaltic melts (Till et al., 2013a) which range from 40–58 km (with uncertainties of 5 km). Moreover, the Sp phase is likely produced by a velocity gradient over a finite depth range, where the nominal depth of the phase defined by its peak amplitude would lie at the depth range mid-point. If the velocity gradient occurred over 20 km, it could span depths as shallow as 45 km, without even considering uncertainties; therefore, the observed Sp phase depths agree with a model in which the basaltic melts are derived from magmas that collected near the base of the lithosphere.

Compared to the Ps migration image of Chen et al. (2013), the Sp CCP stack shows a much stronger and more continuous negative phase in the LAB depth range. A possible explanation for

this discrepancy is that the longer wavelengths of the Sp phases allow them to detect more gradual velocity gradients than the shorter period Ps phases. Alternatively, differences between the Sp and Ps images may reflect their different sensitivities to velocity anisotropy in the mantle, for example the high amplitude, uniform azimuthal anisotropy beneath the High Lava Plain reflected in teleseismic shear-wave splitting (Long et al., 2009). Future work will investigate these possibilities.

3.2.2. Yellowstone and the Snake River Plain

In contrast to other recently tectonized regions, the most striking feature beneath the youngest Yellowstone calderas is the absence of a significant negative Sp phase. Cross-section F–F' (Fig. 7) starts in the Owyhee Plateau, where Sp path density is reasonably good and a robust, perhaps double phase is observed. Continuing through the older Snake River Plain, a negative phase in the potential LAB depth range appears in the CCP stack, but path density is in general low, and the strongest and shallowest segments of this LAB phase (210 km and 340 km along the profile at 60 km depth) correspond to particularly sparse coverage and are not to be trusted (Figs. 4 and 7). Between the 4 Ma and 2 Ma silicic magmas (470 to 520 in profile F–F'), data density is locally high and a

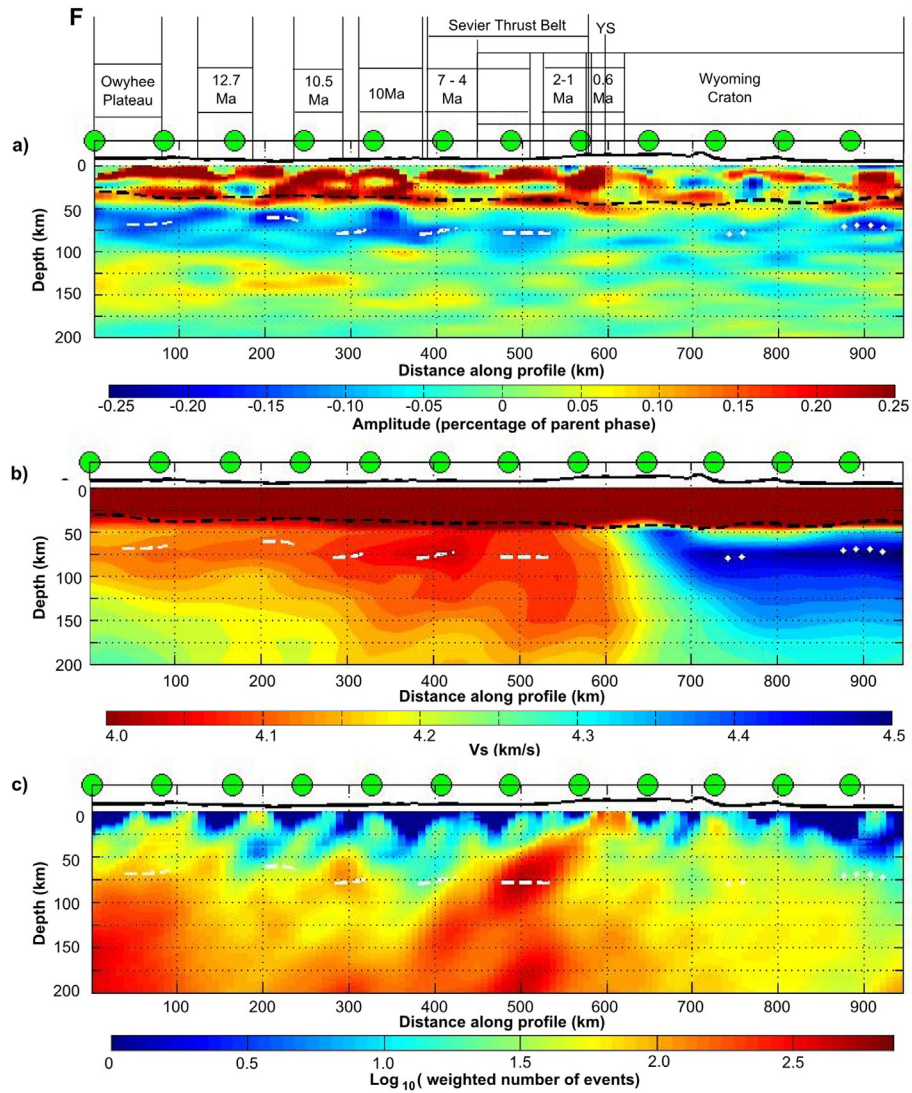


Fig. 7. a) Cross-section F–F' through mean of bootstrapped Sp CCP stack (4–33 s). b) Corresponding cross-section through the tomography model of Obrebski et al. (2011). c) Cross-section of the weighted number of phases contributing to the image. Cross-section runs from 41.7° N, 117.0° W to 46.0° N, 106.8° W (F–F' in Fig. 1). Thick black line: topography, at 5× vertical exaggeration. Dashed black line: Moho (Lowry and Pérez-Gussinyé, 2011). Dashed white line: auto-picked negative phase, interpreted as LAB. Dotted white line: auto-picked negative phase, interpreted as MLD.

robust negative phase appears at depths of 75–100 km; its amplitude is lower than the LAB observed beneath the High Lava Plains and Basin and Range. Beneath the youngest and currently active calderas (550 km to 600 km along profile F–F'), the negative phase disappears completely. This finding differs from the Sp images of Levander and Miller (2012) and Kumar et al. (2012).

A possible interpretation for the lack of an LAB phase beneath Yellowstone is that elevated temperatures and associated partial melts have warmed and infiltrated the lithosphere, obliterating the high velocity lid, as we suggested for the Cascades arc. Tomography models showing very low velocities all the way up to the Moho beneath the Snake River Plain (e.g. Obrebski et al., 2011; Wagner et al., 2010) (Fig. 7) support this interpretation, as does rheological modeling that indicates that the lower crust is less viscous beneath Yellowstone than in surrounding areas, a finding that was attributed to the presence of fluid and/or melt (Chang et al., 2013).

3.2.3. Owyhee Plateau and Grouse Creek Block

The Owyhee Plateau has been interpreted to be Precambrian lithosphere that was further depleted by flood basalt volcanism. It remained relatively undeformed through Miocene extension in the

western United States, with volcanism restricted largely to its margins. These observations have been attributed to a core of strong, depleted lithosphere (Shoemaker, 2004). The crust of the Owyhee Plateau is anomalously thick (Eagar et al., 2011) and has high velocities (Hanson-Hedgecock et al., 2012).

We note subtle differences in the lithosphere on and off of the Owyhee Plateau. The negative Sp phase is observed to broaden and deepen beneath the Owyhee Plateau (Figs. 6 and 7) with two distinct phases at 65 km and 80 km depth (Fig. 6 in particular). When the negative phase is auto-picked (Fig. 4), its depth is locally deeper beneath the center of the Owyhee Plateau, similar to the deeper LAB observed beneath the central portion of the Colorado Plateau (Kumar et al., 2012; Lekic and Fischer, 2014; Levander and Miller, 2012; Levander et al., 2011). However, the persistence of the deeper negative phase to the southeast beneath the Snake River Plain calls the distinctiveness of the Owyhee Plateau lithosphere into question (Fig. 7).

LAB depth also appears to increase to the east across the Sr 0.706 isopleth line into the Phanerozoically re-worked Archean Grouse Creek Block (Fig. S3) south of the Snake River Plain (Fig. 3c). However, paths are relatively sparse in the Grouse Creek Block to the east of 116° W (Fig. 2).

3.3. The base of the low velocity zone

In portions of the study region, a positive Sp phase, indicating a velocity increase with depth, appears within the depth range where velocities increase with depth from their minimum in the asthenospheric low velocity zone seen in tomography models (e.g. Obrebski et al., 2011; Wagner et al., 2010). The localized velocity change necessary to create such a phase would require volatile content, melt fraction or grain size to change rapidly with depth. The mantle beneath the High Lava Plains provides one of the clearest examples (distances of 150 km to 500 km in Fig. 6): positive Sp arrivals at 110 km to 150 km depth, albeit weaker and more diffuse than the LAB phase, follow the southeastward deepening of the base of the low velocity zone in the Obrebski et al. (2011) tomography. Other examples include the Owyhee Plateau and older Snake River Plain (distances of 0 km to 300 km in Fig. 7). These observations suggest that the positive velocity gradient at the base of the asthenospheric low velocity zone is in places more localized in depth than it appears in the tomographic models.

3.4. The origins of the LAB

The distinct differences between shallow mantle discontinuities observed beneath the more recently tectonized portions of the northwestern U.S. and those observed within the Wyoming craton have significant implications for the physical and chemical factors that give rise to the drop in seismic velocity across the seismological LAB.

Beneath much of the Wyoming craton and the westernmost edge of the cratonic mantle beneath the Great Plains, the absence of an Sp phase from the tomographically-defined LAB depth range indicates that the drop in velocity from the cratonic lithosphere to the mantle beneath must occur over ~ 50 km or more (e.g. Ford et al., 2010; Rychert et al., 2007), so it could be as gradual as this gradient appears in the tomography models (e.g. Fig. 7). Velocity gradients over these broad depth ranges can be entirely attributed to the effects of temperature and pressure alone (e.g. Faul and Jackson, 2005; Stixrude and Lithgow-Bertelloni, 2005), although gradual gradients in other properties cannot be ruled out. Where weak, intermittent sub-cratonic LAB Sp phases are observed, they suggest localized sharpening of negative shear velocity gradients over vertical spatial scales of ~ 30 km or less, perhaps due to variations in bulk composition, volatile content, grain size or melt.

Turning to the western and tectonically active portion of our study region, the relatively well-known magmatic history of the High Lava Plains, Columbia River Basalts and Snake River Plain make this a particularly interesting area in which to test models for the origins of the LAB. Due to their higher Sp path densities and more robust Sp LAB phases (Figs. 2, 5 and 7), we use the transition in LAB depth between the eastern High Lava Plains (LAB at 60–65 km) and the northern lobe of the Columbia River Basalts to their north (LAB at 70–80 km) to test two models. We restrict our analysis to the eastern High Lava Plains because we wish to compare model predictions against observations of equilibration depths and temperatures of anhydrous magmas; nominally anhydrous samples were collected largely from the Diamond and Jordan craters in the eastern High Lava Plains (Till et al., 2013a). In the first model, we assume that the lithospheric mantle has higher shear velocities because it has been dehydrated and depleted by partial melting relative to a more hydrated and fertile asthenosphere (e.g. Hirth and Kohlstedt, 1996), and that LAB depth variations represent differences in mechanical deformation. In the second model, we assume that the seismological LAB is defined by mantle solidi and represents the top of a melt-rich layer.

The simplest models of mechanical deformation, ones in which a layer of dry, depleted lithosphere has a constant initial thick-

ness and LAB depth variations represent differences in net pure shear extension, do not appear to be consistent with observed LAB depth variations. Extension in the High Lava Plains has been estimated at 17% from paleomagnetic data (Wells and Heller, 1988) and 16% based on crustal thickness estimates (Eagar et al., 2011). If lithospheric extension beneath the northern Columbia River Basalts was $\sim 0\%$, and the entire region had an initial lithospheric thickness of 70 km, 16–17% extension beneath the High Lava Plains could explain much of the observed LAB depth offset (e.g. an LAB at 60 km beneath the High Lava Plains versus an LAB at 70 km beneath the northern Columbia River Basalts). However, this model fails on a broader basis. In regions of the northern Basin Range where extension has been estimated at 50% (McQuarrie and Wernicke, 2005), averaged LAB depths lie no shallower than ~ 65 km to 70 km (Lekic and Fischer, 2014). Had 70 km thick lithosphere undergone 50% extension by simple pure shear stretching (e.g. McKenzie, 1978), we would instead expect the lithosphere to be less than 50 km thick.

Models in which the negative LAB velocity gradient is created by an increase in partial melt above the solidus do appear to be plausible. In such a model, partial melt generated at a range of depths in the asthenosphere buoyantly rises to collect in a layer whose upper boundary is defined by the solidus for that melt composition. Although estimates of partial melt volumes generated at any point in the oceanic asthenosphere may be too small to produce a significant reduction in shear velocity (Hirschmann, 2010; Karato, 2012), data from the High Lava Plains indicate 5–13% batch melting is occurring, generating enough partial melt to produce the required shear velocity gradient (Till et al., 2013b). In addition, given that the pressure dependences of basaltic melt viscosity and density suggest rapid melt migration out of the depth range 90–150 km (Sakamaki et al., 2013), melt should tend to collect in the depth range in which we observe an LAB phase to the west of the Sevier Thrust Belt (50–80 km). Rising above the depth of its solidus, melt will tend to solidify rapidly; melt could also be inhibited from rising to shallower depths by a permeability barrier (Hirschmann, 2010; Till et al., 2010). Some melt must still be able to make its way to the surface to produce the very young samples observed in the High Lava Plains (Till et al., 2013a), but not in the northern Columbia River Basalt region.

With a solidus-defined model and comparable asthenospheric compositions, the ~ 10 km shallower depth of the seismological LAB beneath the High Lava Plains indicates higher mantle temperatures, a reasonable inference given the High Lava Plains' active magmatism compared to magmatic quiescence in the northern Columbia River Basalts since 15 Ma, and the relatively low mantle shear velocities observed beneath the High Lava Plains (e.g. Obrebski et al., 2011 in Fig. 5). In one scenario, the geodynamic model of Kincaid et al. (2013) shows that interactions between subducting lithosphere and a mantle plume can predict the timing of magmatism in the region. In this model, present-day temperatures at the base of the North American plate are up to 100 °C higher beneath the High Lava Plains than the northern Columbia River Basalts.

Candidate geotherms for the eastern High Lava Plains and northern Columbia River Basalts illustrate the deeper geotherm-solidus intersection in the latter region. Peridotite solidi with 0–200 ppm water were assumed (Hirschmann et al., 2009), in keeping with the relatively anhydrous young basaltic magmas in the eastern High Lava Plains (Till et al., 2013a). A present-day High Lava Plains geotherm is required to 1) intersect the temperatures and pressures of last equilibration for the young basalts (Till et al., 2013a) and 2) to cross the peridotite solidi such that melt would begin to solidify at depths overlapping with the negative velocity gradient imaged by the Sp phases (60 km \pm 10 km for the eastern High Lava Plains, assuming a velocity gradient over 20 km centered

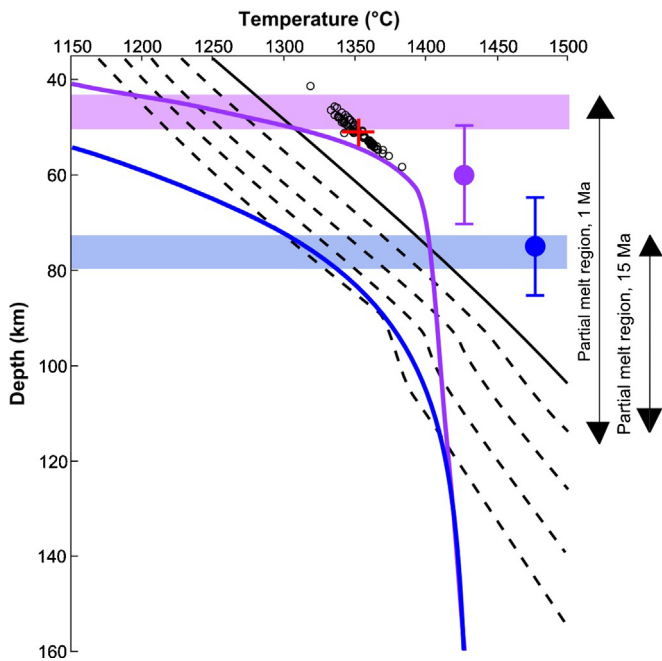


Fig. 8. Shallowing of the top of a melt-rich layer with younger, hotter geotherm. Black solid line: dry peridotite solidus; dashed black lines: damp peridotite solidi, with water content increasing in 50 ppm increments from 50 to 200 ppm (Hirschmann et al., 2009; Hirschmann, 2000). Purple solid line: candidate High Lava Plains geotherm for a mantle potential temperature of 1380 °C that has cooled for 1 My. Blue solid line: candidate northern Columbia River Basalts geotherm for the same conditions except with cooling over 15 My. Crustal thickness is 37 km (Eagar et al., 2011); crustal heat production is $0.93 \mu\text{W m}^{-3}$ (typical for continental crust; Rudnick and Fountain, 1995); initial surface heat flow is 95 mW m^{-2} (the upper end of values currently observed in High Lava Plains; Blackwell et al., 1982); heat flow at infinite time is 40 mW m^{-2} ; thermal conductivity is $2.7 \text{ W m}^{-1} \text{ }^\circ\text{C}^{-1}$ (typical for oceanic lithosphere; Hofmeister, 1999). Purple and blue shaded regions show the top of the region where partial melt is stable for the 1 My and 15 My geotherms, respectively. Arrows adjacent to figure show the entire extent of the partial melt region. Purple and blue circles show representative LAB velocity gradient depths observed in this study for the High Lava Plains and the northern Columbia River Basalts, respectively, assuming LAB velocity gradients are distributed over 20 km. Black circles: basalt magma equilibration temperatures in the eastern High Lava Plains (Till et al., 2013a); red bars show the mean and standard deviation of these samples ($1353 \text{ }^\circ\text{C} \pm 11 \text{ }^\circ\text{C}$ and $51 \text{ km} \pm 3 \text{ km}$). (For interpretation of the references to color in this figure legend, the reader is referred to the web version of this article.)

on the average depth of the phase). A geotherm for 37 km thick continental crust (Eagar et al., 2011) with a mantle potential temperature of 1380 °C that has cooled over 1 My meets these criteria (Fig. 8). With 15 My of cooling, the geotherm intersects the solidi in a depth range that intersects the Sp LAB velocity gradient for the northern Columbia River Basalts ($75 \text{ km} \pm 10 \text{ km}$). The equilibration ages of the geotherms are chosen to coincide with the timing of major magmatic events that may correspond to high temperature conditions in these areas. Newberry Volcano, the most recent major silicic crater of the High Lava Plains trend, dates to 1 Ma (Till et al., 2013a); whereas the major outpouring of Columbia River Basalts ended 15 Ma (Hooper et al., 2002). These simple conductive geotherms are not intended to precisely represent the thermal history of the region, which is almost certainly more complex. However, they do show that a time-dependent solidus-based model for the LAB is capable of explaining the LAB depth variations observed between the High Lava Plains and the northern Columbia River Basalts.

4. Conclusions

Three-dimensional imaging with CCP stacking of Sp phases reveals strong variations in shallow mantle discontinuity structure

across the northwestern United States over different spatial scales and tectonic time scales.

A coherent Sp phase that coincides with the LAB depth range in tomographic models is observed throughout the region to the west of the Sevier Thrust Belt, south of 45° N. In contrast, beneath stable cratonic regions, an Sp phase is typically absent at LAB depths, indicating that the negative LAB velocity gradient is gradual enough (distributed over >50 km) to be consistent with a purely thermal gradient; the presence of weak, intermittent Sp phases in the cratonic LAB depth range suggests localized sharpening of the LAB velocity gradient over vertical spatial scales of ~30 km or less, perhaps due to variations in bulk composition, volatile content, grain size or melt. MLDs exist within the cratonic mantle lithosphere and are often distributed in depth, but in places only a single MLD appears.

A ~10 km deepening of the LAB occurs at the transition between the High Lava Plains (with its <10 Ma magmatism) and the >15 Ma Columbia River Basalts to the north. This variation and observed melt equilibration temperatures and pressures (Till et al., 2013a) are consistent with a model in which a strong negative LAB velocity gradient is created by the presence of partial melt collected below a solidus-defined boundary. Underneath the Yellowstone Caldera, the LAB discontinuity disappears; there high melt volumes and elevated temperatures may have so completely permeated the lithosphere as to obliterate any LAB velocity contrast.

A positive Sp phase observed at depths consistent with the base of the asthenospheric low velocity zone suggests that this velocity gradient may be locally sharp.

Acknowledgements

Waveform data were obtained from the IRIS Data Management Center. Thanks to M. Obrebski for the tomographic models of Obrebski et al. (2010, 2011) and to C. Till for helpful discussion. We also thank P. Shearer, M. Hirschmann and an anonymous reviewer for their comments. This research was supported by the NSF EarthScope Program through award EAR-0844276.

Appendix A. Supplementary material

Supplementary material related to this article can be found online at <http://dx.doi.org/10.1016/j.epsl.2013.12.016>.

References

- Abt, D.L., Fischer, K.M., French, S.W., Ford, H.A., Yuan, H., Romanowicz, B., 2010. North American lithospheric discontinuity structure imaged by Ps and Sp receiver functions. *J. Geophys. Res.* 115, B09301.
- Armstrong, R.L., Taubeneck, W.H., Hales, P.O., 1977. Rb–Sr and K–Ar geochronometry of Mesozoic granitic rocks and their Sr isotopic composition, Oregon, Washington, and Idaho. *Geol. Soc. Am. Bull.* 88, 397–411.
- Blackwell, D.D., Bowen, R.G., Hull, D.A., Riccio, J., Steele, J.L., 1982. Heat flow, arc volcanism, and subduction in northern Oregon. *J. Geophys. Res.* 87, 8735–8754.
- Bostock, M.G., 1998. Mantle stratigraphy and evolution of the Slave province. *J. Geophys. Res.* 103, 21183–21200.
- Burdick, S., Hilst, R.D., van der Vernon, F.L., Martynov, V., Cox, T., Eakins, J., Karasu, G.H., Tyell, J., Astiz, L., Pavlis, G.L., 2012. Model update March 2011: Upper mantle heterogeneity beneath North America from traveltimes tomography with global and USArray Transportable Array data. *Seismol. Res. Lett.* 83, 23–28.
- Camp, V.E., Ross, M.E., 2004. Mantle dynamics and genesis of mafic magmatism in the intermontane Pacific Northwest. *J. Geophys. Res.* 109, B08204.
- Camp, V.E., Ross, M.E., Hanson, W.E., 2003. Genesis of flood basalts and Basin and Range volcanic rocks from Steens Mountain to the Malheur River Gorge, Oregon. *Geol. Soc. Am. Bull.* 115, 105–128.
- Canil, D., 2004. Mildly incompatible elements in peridotites and the origins of mantle lithosphere. *Lithos* 77, 375–393.
- Canil, D., 2008. Canada's craton: A bottoms-up view. *GSA Today* 18 (6), 4.
- Chang, W.-L., Smith, R.B., Puskas, C.M., 2013. Effects of lithospheric viscoelastic relaxation on the contemporary deformation following the 1959 Mw 7.3 Hebgen

- Lake, Montana, earthquake and other areas of the intermountain seismic belt. *Geochem. Geophys. Geosyst.* 14, 1–17.
- Chen, C.-W., James, D.E., Fouch, M.J., Wagner, L.S., 2013. Lithospheric structure beneath the High Lava Plains, Oregon, imaged by scattered teleseismic waves. *Geochem. Geophys. Geosyst.* 14, 4835–4848. <http://dx.doi.org/10.1002/ggge.20284>.
- Christiansen, R.L., Foulger, G.R., Evans, J.R., 2002. Upper-mantle origin of the Yellowstone hotspot. *Geol. Soc. Am. Bull.* 114, 1245–1256.
- Coney, P.J., Jones, D.L., Monger, J.W.H., 1980. Cordilleran suspect terranes. *Nature* 288, 329–333.
- Cooper, C.M., Lenardic, A., Moresi, L., 2004. The thermal structure of stable continental lithosphere within a dynamic mantle. *Earth Planet. Sci. Lett.* 222, 807–817.
- Darold, A., Humphreys, E., 2013. Upper mantle seismic structure beneath the Pacific Northwest: A plume-triggered delamination origin for the Columbia River flood basalt eruptions. *Earth Planet. Sci. Lett.* 365, 232–242.
- DeCelles, P.G., Coogan, J.C., 2006. Regional structure and kinematic history of the Sevier fold-and-thrust belt, central Utah. *Geol. Soc. Am. Bull.* 118, 841–864.
- Dickinson, W.R., 2004. Evolution of the North American Cordillera. *Annu. Rev. Earth Planet. Sci.* 32, 13–45.
- Druken, K.A., Long, M.D., Kincaid, C., 2011. Patterns in seismic anisotropy driven by rollback subduction beneath the High Lava Plains. *Geophys. Res. Lett.* 38, L13310.
- Eagar, K.C., Fouch, M.J., James, D.E., Carlson, R.W., 2011. Crustal structure beneath the High Lava Plains of eastern Oregon and surrounding regions from receiver function analysis. *J. Geophys. Res.* 116, 141–153.
- Faccenna, C., Becker, T.W., Lallemand, S., Lagabrielle, Y., Funicello, F., Piromallo, C., 2010. Subduction-triggered magmatic pulses: A new class of plumes? *Earth Planet. Sci. Lett.* 299, 54–68.
- Faul, U.H., Jackson, I., 2005. The seismological signature of temperature and grain size variations in the upper mantle. *Earth Planet. Sci. Lett.* 234, 119–134.
- Fenneman, N.M., Johnson, D.W., 1946. Physical divisions of the United States: US geological survey map prepared in cooperation with the physiographic commission. *U.S. Geol. Surv.*, scale 1:7,000,000.
- Ford, H.A., Fischer, K.M., Abt, D.L., Rychert, C.A., Elkins-Tanton, L.T., 2010. The lithosphere–asthenosphere boundary and cratonic lithospheric layering beneath Australia from Sp wave imaging. *Earth Planet. Sci. Lett.* 300, 299–310.
- Ford, M.T., Grunder, A.L., Duncan, R.A., 2013. Bimodal volcanism of the High Lava Plains and northwestern Basin and Range of Oregon: The distribution and tectonic implications of age-progressive rhyolites. *Geochem. Geophys. Geosyst.* 14, 2836–2857. <http://dx.doi.org/10.1002/ggge.20175>.
- Foster, D.A., Mueller, P.A., Mogk, D.W., Wooden, J.L., Vogl, J.J., 2006. Proterozoic evolution of the western margin of the Wyoming craton: implications for the tectonic and magmatic evolution of the northern Rocky Mountains. *Can. J. Earth Sci.* 43, 1601–1619.
- Fouch, M.J., 2012. The Yellowstone hotspot: Plume or not? *Geology* 40, 479–480.
- Gao, H., Shen, Y., 2014. Upper mantle structure of the Cascades from full-wave ambient noise tomography: Evidence for 3D mantle upwelling in the back arc. *Earth Planet. Sci. Lett.* 390, 222–233.
- Gaschnig, R.M., Vervoort, J.D., Lewis, R.S., Tikoff, B., 2011. Isotopic evolution of the Idaho batholith and Challis intrusive province, Northern US Cordillera. *J. Petrol.* 52, 2397–2429.
- Hansen, S.M., Dueker, K.G., Stachnik, J.C., Aster, R.C., Karlstrom, K.E., 2013. A rootless Rockies – Support and lithospheric structure of the Colorado Rocky mountains inferred from CREST and TA seismic data. *Geochem. Geophys. Geosyst.* 14, 2670–2697. <http://dx.doi.org/10.1002/ggge.20143>.
- Hanson-Hedgecock, S., Wagner, L.S., Fouch, M.J., James, D.E., 2012. Constraints on the causes of mid-Miocene volcanism in the Pacific Northwest US from ambient noise tomography. *Geophys. Res. Lett.* 39.
- Helffrich, G., 2006. Extended-time multitaper frequency domain cross-correlation receiver-function estimation. *Bull. Seismol. Soc. Am.* 96, 344–347.
- Hirschmann, M.M., 2000. Mantle solidus: Experimental constraints and the effects of peridotite composition. *Geochem. Geophys. Geosyst.* 1, 1042.
- Hirschmann, M.M., 2010. Partial melt in the oceanic low velocity zone. *Phys. Earth Planet. Inter.* 179 (1), 60–71.
- Hirschmann, M.M., Tenner, T., Aubaud, C., Withers, A.C., 2009. Dehydration melting of nominally anhydrous mantle: The primacy of partitioning. *Phys. Earth Planet. Inter.* 176, 54–68.
- Hirth, G., Kohlstedt, D.L., 1996. Water in the oceanic upper mantle: implications for rheology, melt extraction and the evolution of the lithosphere. *Earth Planet. Sci. Lett.* 144, 93–108.
- Hofmeister, A.M., 1999. Mantle values of thermal conductivity and the geotherm from phonon lifetimes. *Science* 283 (5408), 1699–1706.
- Hooper, P.R., Binger, G.B., Lees, K.R., 2002. Ages of the Steens and Columbia River flood basalts and their relationship to extension-related calc-alkalic volcanism in eastern Oregon. *Geol. Soc. Am. Bull.* 114, 43–50.
- James, D.E., Fouch, M.J., Carlson, R.W., Roth, J.B., 2011. Slab fragmentation, edge flow and the origin of the Yellowstone hotspot track. *Earth Planet. Sci. Lett.* 311, 124–135.
- Jordan, B.T., Grunder, A.L., Duncan, R.A., Deino, A.L., 2004. Geochronology of age-progressive volcanism of the Oregon High Lava Plains: Implications for the plume interpretation of Yellowstone. *J. Geophys. Res.* 109, B10202.
- Karato, S., 2012. On the origin of the asthenosphere. *Earth Planet. Sci. Lett.* 321–322, 95–103.
- Kelemen, P.B., Hart, S.R., Bernstein, S., 1998. Silica enrichment in the continental upper mantle via melt/rock reaction. *Earth Planet. Sci. Lett.* 164, 387–406.
- Kennett, B.L.N., 1991. The removal of free surface interactions from three-component seismograms. *Geophys. J. Int.* 104, 153–163.
- Kincaid, C., Druken, K.A., Griffiths, R.W., Stegman, D.R., 2013. Bifurcation of the Yellowstone plume driven by subduction-induced mantle flow. *Nat. Geosci.* 6, 395–399.
- Kumar, P., Kind, R., Yuan, X., Mechie, J., 2012. USArray receiver function images of the lithosphere–asthenosphere boundary. *Seismol. Res. Lett.* 83, 486–491.
- Lee, C.-T.A., 2006. Geochemical/petrologic constraints on the origin of cratonic mantle. In: Benn, K., Mareschal, J.-C., Condie, K.C. (Eds.), *Archean Geodynamics and Environments*. In: *Geophys. Monogr.*, vol. 164. AGU, Washington, DC, pp. 89–114.
- Lee, C.-T.A., Luffi, P., Chin, E.J., 2011. Building and destroying continental mantle. *Annu. Rev. Earth Planet. Sci.* 39, 59–90.
- Lekic, V., Fischer, K., 2014. Contrasting lithospheric signatures across the western United States revealed by Sp receiver functions. *Earth Planet. Sci. Lett.* 402, 90–98. <http://dx.doi.org/10.1016/j.epsl.2013.11.026> (in this volume).
- Lekic, V., French, S.W., Fischer, K.M., 2011. Lithospheric thinning beneath rifted regions of Southern California. *Science* 334, 783–787.
- Levander, A., Miller, M.S., 2012. Evolutionary aspects of lithosphere discontinuity structure in the western U.S. *Geochem. Geophys. Geosyst.* 13, Q0AK07.
- Levander, A., Schmandt, B., Miller, M.S., Liu, K., Karlstrom, K.E., Crow, R.S., Lee, C.-T.A., Humphreys, E.D., 2011. Continuing Colorado plateau uplift by delamination-style convective lithospheric downwelling. *Nature* 472, 461–465.
- Li, X., Yuan, X., Kind, R., 2007. The lithosphere–asthenosphere boundary beneath the western United States. *Geophys. J. Int.* 170, 700–710.
- Lin, F.-C., Ritzwoller, M.H., Yang, Y., Moschetti, M.P., Fouch, M.J., 2011. Complex and variable crustal and uppermost mantle seismic anisotropy in the western United States. *Nat. Geosci.* 4, 55–61.
- Liu, L., Stegman, D.R., 2012. Origin of Columbia River flood basalt controlled by propagating rupture of the Farallon slab. *Nature* 482, 386–389.
- Long, M.D., Gao, H., Klaus, A., Wagner, L.S., Fouch, M.J., James, D.E., Humphreys, E., 2009. Shear wave splitting and the pattern of mantle flow beneath eastern Oregon. *Earth Planet. Sci. Lett.* 288, 359–369.
- Long, M.D., Till, C.B., Druken, K.A., Carlson, R.W., Wagner, L.S., Fouch, M.J., James, D.E., Grove, T.L., Schmerr, N., Kincaid, C., 2012. Mantle dynamics beneath the Pacific Northwest and the generation of voluminous back-arc volcanism. *Geochem. Geophys. Geosyst.* 13, Q0AN01.
- Lowry, A.R., Pérez-Gussinyé, M., 2011. The role of crustal quartz in controlling Cordilleran deformation. *Nature* 471, 353–357.
- McCroxy, P.A., Blair, J.L., Oppenheimer, D.H., Walter, S.R., 2006. Depth to the Juan de Fuca slab beneath the Cascadia subduction margin: A 3D model for sorting earthquakes. *U.S. Geol. Surv. Digit. Data Ser.* 91. Version 1.2.
- McKenzie, D., 1978. Some remarks on the development of sedimentary basins. *Earth Planet. Sci. Lett.* 40 (1), 25–32.
- McQuarrie, N., Wernicke, B.P., 2005. An animated tectonic reconstruction of southwestern North America since 36 Ma. *Geosphere* 1, 147–172.
- Mercier, J.-P., Bostock, M.G., Audet, P., Gaherty, J.B., Garnero, E.J., Revenaugh, J., 2008. The teleseismic signature of fossil subduction: Northwestern Canada. *J. Geophys. Res.* 113, B04308.
- Obrebski, M., Allen, R.M., Xue, M., Hung, S.-H., 2010. Slab-plume interaction beneath the Pacific Northwest. *Geophys. Res. Lett.* 37, L14305.
- Obrebski, M., Allen, R.M., Pollitz, F., Hung, S.-H., 2011. Lithosphere–asthenosphere interaction beneath the western United States from the joint inversion of body-wave traveltimes and surface-wave phase velocities. *Geophys. J. Int.* 185, 1003–1021.
- Parman, S.W., Grove, T.L., Dann, J.C., de Wit, M.J., 2004. A subduction origin for komatiites and cratonic lithospheric mantle. *S. Afr. J. Geol.* 107, 107–118.
- Pierce, K.L., Morgan, L.A., 1992. The track of the Yellowstone hotspot: Volcanism, faulting, and uplift. In: Link, P.K., Kuntz, M.A., Platt, L.B. (Eds.), *Regional Geology of Eastern Idaho and Western Wyoming*. In: *GSA Mem.*, vol. 179, pp. 1–53.
- Pierce, K.L., Morgan, L.A., 2009. Is the track of the Yellowstone hotspot driven by a deep mantle plume? – Review of volcanism, faulting, and uplift in light of new data. *J. Volcanol. Geotherm. Res.* 188, 1–25.
- Rudnick, R.L., Fountain, D.M., 1995. Nature and composition of the continental crust: a lower crustal perspective. *Rev. Geophys.* 33, 267–309.
- Rychert, C.A., Rondenay, S., Fischer, K.M., 2007. P-to-S and S-to-P imaging of a sharp lithosphere–asthenosphere boundary beneath eastern North America. *J. Geophys. Res.* 112, B08314.
- Sakamaki, T., Suzuki, A., Ohtani, E., Terasaki, H., Urakawa, S., Katayama, Y., Funakoshi, K.-I., Wang, Y., Hernlund, J., Ballmer, M.D., 2013. Ponded melt at the boundary between the lithosphere and asthenosphere. *Nat. Geosci.* 6, 1041–1044.
- Saleeby, J., 2003. Segmentation of the Laramide Slab—evidence from the southern Sierra Nevada region. *Geol. Soc. Am. Bull.* 115, 655–668.

- Schmandt, B., Humphreys, E., 2010. Complex subduction and small-scale convection revealed by body-wave tomography of the western United States upper mantle. *Earth Planet. Sci. Lett.* 297, 435–445.
- Schmandt, B., Dueker, K., Humphreys, E., Hansen, S., 2012. Hot mantle upwelling across the 660 beneath Yellowstone. *Earth Planet. Sci. Lett.* 331–332, 224–236.
- Sheehan, A.F., Shearer, P.M., Gilbert, H.J., Dueker, K.G., 2000. Seismic migration processing of P-SV converted phases for mantle discontinuity structure beneath the Snake River Plain, western United States. *J. Geophys. Res.* 105, 19055–19065.
- Shen, W., Ritzwoller, M.H., Schulte-Pelkum, V., 2013. A 3-D model of the crust and uppermost mantle beneath the Central and Western US by joint inversion of receiver functions and surface wave dispersion. *J. Geophys. Res.* 118, 262–276.
- Shervais, J.W., Hanan, B.B., 2008. Lithospheric topography, tilted plumes, and the track of the Snake River–Yellowstone hot spot. *Tectonics* 27, 51–54.
- Shoemaker, K.A., 2004. The tectonomagmatic evolution of the Late Cenozoic Owyhee Plateau, northwestern United States. Dissertation thesis. Miami Univ., Oxford, Ohio, 288 pp.
- Sigloch, K., 2011. Mantle provinces under North America from multifrequency P wave tomography. *Geochem. Geophys. Geosyst.* 12.
- Simon, N.S.C., Carlson, R.W., Pearson, D.G., Davies, G.R., 2007. The origin and evolution of the Kaapvaal cratonic lithospheric mantle. *J. Petrol.* 48, 589–625.
- Smith, R.B., Jordan, M., Steinberger, B., Puskas, C.M., Farrell, J., Waite, G.P., Husen, S., Chang, W.-L., O'Connell, R., 2009. Geodynamics of the Yellowstone hotspot and mantle plume: Seismic and GPS imaging, kinematics, and mantle flow. *J. Volcanol. Geotherm. Res.* 188, 26–56.
- Snyder, D.B., 2008. Stacked uppermost mantle layers within the Slave craton of NW Canada as defined by anisotropic seismic discontinuities. *Tectonics* 27, TC4006.
- Stixrude, L., Lithgow-Bertelloni, C., 2005. Mineralogy and elasticity of the oceanic upper mantle: Origin of the low-velocity zone. *J. Geophys. Res.* 110, 610–632.
- Tikoff, B., Maxson, J., 2001. Lithospheric buckling of the Laramide foreland during Late Cretaceous and Paleogene, western United States. *Rocky Mt. Geol.* 36, 13–35.
- Till, C.B., Elkins-Tanton, L.T., Fischer, K.M., 2010. A mechanism for low-extent melts at the lithosphere–asthenosphere boundary. *Geochem. Geophys. Geosyst.* 11, Q10015. <http://dx.doi.org/10.1029/2010GC003234>.
- Till, C.B., Grove, T.L., Carlson, R.W., Donnelly-Nolan, J.M., Fouch, M.J., Wagner, L.S., Hart, W.K., 2013a. Depths and temperatures of <10.5 Ma mantle melting and the lithosphere–asthenosphere boundary below southern Oregon and northern California. *Geochem. Geophys. Geosyst.* 14 (4), 864–879.
- Till, C.B., Grove, T., Donnelly-Nolan, J., Carlson, R., 2013b. Depths and temperatures of mantle melt extraction in the Southern Cascadia subduction zone. Abstract S11C-07 Presented at 2013 Fall Meeting, AGU, San Francisco, Calif., 9–13 Dec.
- Wagner, L., Forsyth, D.W., Fouch, M.J., James, D.E., 2010. Detailed three-dimensional shear wave velocity structure of the northwestern United States from Rayleigh wave tomography. *Earth Planet. Sci. Lett.* 299, 273–284.
- Wells, R.E., Heller, P.L., 1988. The relative contribution of accretion, shear, and extension to Cenozoic tectonic rotation in the Pacific Northwest. *Geol. Soc. Am. Bull.* 100, 325–338.
- Wilson, D.C., Angus, D.A., Ni, J.F., Grand, S.P., 2006. Constraints on the interpretation of S-to-P receiver functions. *Geophys. J. Int.* 165, 969–980.
- Yuan, H., Romanowicz, B., 2010a. Lithospheric layering in the North American craton. *Nature* 466, 1063–1068.
- Yuan, H., Romanowicz, B., 2010b. Depth dependent azimuthal anisotropy in the western US upper mantle. *Earth Planet. Sci. Lett.* 300, 385–394.
- Yuan, H., Romanowicz, B., Fischer, K.M., Abt, D., 2011. 3-D shear wave radially and azimuthally anisotropic velocity model of the North American upper mantle. *Geophys. J. Int.* 184, 1237–1260.